# Geometric Decoupling of a Mouse Array Coil Using a Dual Plane Pair Design with Crisscrossed Return Paths and Custom Mounting Fixture*

Wen-Yang Chiang, *Member, IEEE*, and Mary P. McDougall, *Member, IEEE*

*Abstract*— **An element design for receive array coils that decouples from the transmit coil without external active detuning is presented for magnetic resonance imaging (MRI) of mice. The array element uses a crisscrossed geometry on the return paths to reduce the current induced by the transmit coil. Without the need for an external active detune network, the proposed method simplifies the construction of MRI coil systems and also mitigates problems in space-limited MRI applications. In addition, an adaptable scissor-jack-like fixture is presented that allows the receive array to move parallel to the transmit coil to maintain the decoupling condition while maintaining close contact with varying sizes of mice.**

## I. Introduction

The mouse continues to grow in importance as the laboratory animal of choice for applications based on pharmacological or surgical interventions used in combination with or without genetic modifications [1]-[3]. Therefore, the need for noninvasive tools for characterizing disease progression or serial assessment of response to intervention follows, and Magnetic Resonance Imaging (MRI) offers all of its traditional benefits over other imaging modalities with regard to contrast and versatility [7]. Depicting the small details of mouse morphology as compared to human, however, presents a challenge to the fundamental capabilities of MRI with regard to maintaining signal to noise ratio (SNR) in high resolution imaging when the voxel size is small. Some of the SNR loss can be recovered through the use of dedicated high-field animal scanners and specialized RF coil design, but much of it must be regained through time-consuming acquisition and averaging of data. Therefore, high resolution MR imaging of mice is generally considered to take on the order of hours.

The use of array coils and accelerated imaging is a natural form of relief to consider, particularly as multiple channel receivers are now ubiquitous and the benefits of parallel imaging have become apparent in the human and murine imaging arena in nearly all applications [5]. Several groups have reported work in developing array coils for imaging mice and rats for clinical-bore-size as well as high field animal scanners [5-12]. In general, researchers note the challenges associated with the miniaturization of the coils, including but not limited to maintaining sample noise dominance, sensitivity in the element-to-element decoupling process, and the lack of space for traditional hardware.

* Research supported by American Heart Association.

The authors are with Department of Biomedical Engineering, Texas A&M University, College Station, TX 77843 USA. (e-mail: wychiang@tamu.edu; mpmcdougall@tamu.edu)

Receive array coils traditionally employ some combination of active and passive detuning configurations in order to decouple from the volume coil during transmit [13], [14]. In space limited situations, however, such as with small bore systems or with arrays intended for use on small samples or animals, this requirement can be difficult to realize simply in terms of real estate. We have previously reported planar pair and dual-plane pair (DPP) element designs that are decoupled from the transmit coil due to their counter-rotating flux paths on either side of the element [15]; however, we have recently noted that for certain element sizes, the loop mode of the receiving element can couple to the volume coil, independent from the imaging mode.

This paper presents a 10-channel array coil with an element design that uses a dual plane pair configuration [15] with "crisscrossed" return paths (DPPX) as the receive element. The design is less sensitive than a loop coil; therefore an adjustable custom fixture is also described that allowed the receive array to maintain close contact with varying sizes of mice while maintaining the decoupling condition in the transmit coil.

## II. Methods

### A. Background of Dual Plane Pair with Crisscrossed Return Path (DPPX)

Our group previously has reported the ability of the DPP element to decouple from the transmit coil without any active detune network due to flux being induced in equal and opposite directions in the two halves of the coil [15], as is illustrated in Fig. 1. During our investigation of applying the DPP coil array to mouse MRI, we found that the loop mode of the DPP coil formed by the return paths caused local signal loss due to coupling when the imaging subject was too close to the DPP array. The DPPX design was designed to alleviate this problem.

### B. Illustration of Loop Mode Effect

To illustrate the issue, we manufactured the traces only (no resonating capacitors) of DPP coils with three different types of return paths: a conventional DPP coil, a DPP trace with shorted return paths (intended to change the size of the loop coupling to the transmit field), and a DPPX coil. The return paths are shown in Fig 2. We placed each type of trace under a cylindrical $CuSO_4$ phantom and imaged each assembly using our birdcage coil which will be described later. The imaging parameters are shown in Table 1.

### C. Quasi-Static Field Simulation

To estimate the radio frequency field strength (B1 field) of the DPPX coil, a straightforward quasi-static approach was used. We assumed the cross sectional area of the conductor compared with the length to be small, and therefore approximated the current flow on the conductor to be on an infinitely thin wire located at the geometric center of the conduction.

The DPPX coil was designed in Eagle software, and the trace pattern was exported to our in-house Biot-Savart routine implemented on MATLAB. The trace of the DPPX coil was first discretized into 1-mil (0.0254 mm) filaments, and current intensity and direction were assigned to each filament to simulate current flow.

We simulated the B1 field of the DPPX coil with currents as shown in Fig 3 enforcing twice the current on the signal line than in the return paths and enforcing 180$^{o}$ phase difference between the signal and return paths.

### D. DPPX coil

The PCB of the DPPX coil was manufactured by Sunstone (Mulino, OR) as shown in Fig. 4(a) and (b). The trace width of the signal line was 30 mil (0.76 mm) and the trace width of the return path was 16 mil (0.41 mm). The width of each crisscrossed loop was 198 mil (5.03 mm), and the length of the signal line was 1855 mil (47.12 mm). In Fig. 4(C), capacitor C1 = 18 pF (Passive Plus, Huntington, NY) was carefully chosen to ensure the difference of current phase between the signal line and the return paths is 180°. To choose the value of C1, we varied the values until there is no null-spot artifact in the MR images. The variable capacitors C2 and C5 (1-5 pF, Johanson Dielectrics, Sylmar, CA) were used for adjusting the tuning and the matching of the DPPX coil.

### E. Adjustable Coil Holder

An adjustable coil holder was designed to accommodate different sizes of mice as shown in Fig 5 The ten DPPX coils were separately placed on two pieces of fixtures—five DPPX coils on the top of the mouse and five on the bottom of the mouse. Each set of the five DPPX coils were arranged on a cylindrical surface with curvature of 0.75" (19.05 mm). To better control the coil-coil interactions and minimize off-centered loading problems, we designed a scissor-jack-like mechanism which lets the top five DPPX coils and the bottom five DPPX coils to be able to move at equal amounts around the center of the birdcage coil. Also, the DPPX array on the top, the DPPX array on the bottom, and the birdcage coil are always parallel to each other in this design. This shows how human cardiac arrays can be applied to mouse-sized arrays while reducing the chance of coupling to other birdcage modes such as end-ring mode. Flexible micro coax (K_01152-07, Huber+Suhner, Switzerland) was also used to allow the coil holder to move without obstruction.

### F. Voltage regulation and pre-amplifier

WanTcom (Chanhassen, MN, USA) pre-amplifiers were used to mitigate coil-to-coil interactions [14]. The preamp was placed perpendicular to the B1 field to increase stability.

TABLE I. MRI PARAMETERS FOR IMAGING THE $CuSO_4$ PHANTOMS AND THE EUTHANIZED MOUSE.

| Parameters | Imaging Protocol | |
|---|---|---|
| | ***Checking loop Mode of Different Kinds of Traces Using $CuSO_4$ Phantom*** | ***Array Imaging of $CuSO_4$ Phantom and Euthanized Mouse*** |
| Sequence | Spin Echo | Spin Echo |
| Echo Time (TE) | 30 msec | 30 msec |
| Repetition Time (TR) | 1000 msec | 1000 msec |
| Field of View (FOV) | 50 mm x 50 mm | 40 mm x 40 mm |
| Matrix Size | 256 x 128 | 256 x 128 |
| Slice Thickness | 1 mm | 1 mm |
| Number of Excitation (NEX) | 1 | 1 |

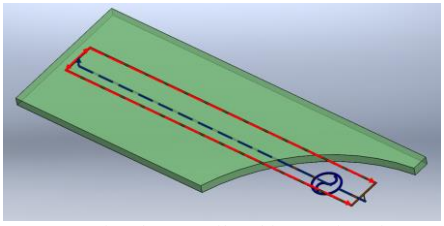

Figure 1. Conventional DPP coil and its quasi-static current flow.


Figure 2. To validate the induced current being cancelled on the return paths of the DPPX coil, we built three trace-only coils without any capacitors. (a) Dual plane pair. (b) Dual plane pair with shorted return paths. (c) Dual plane pair with criss-cross return paths.

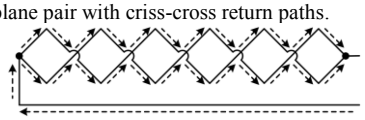

Figure 3. Current directions for the quasi-static simulation.

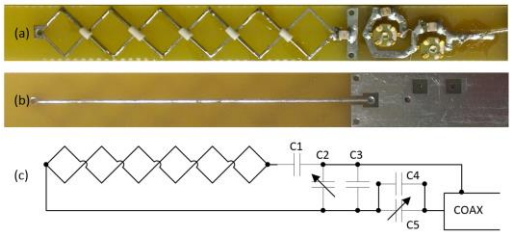


Figure 4. DPPX coil. (a) top (showing the crisscrossed return paths). (b) bottom (showing the signal line). (c) Electric circuit of single DPPX coil. The coil is tuned by C2 and C3 and matched by C4. The value of C1 was carefully chosen to make sure the current phase between the return paths and the signal line to be 180°.

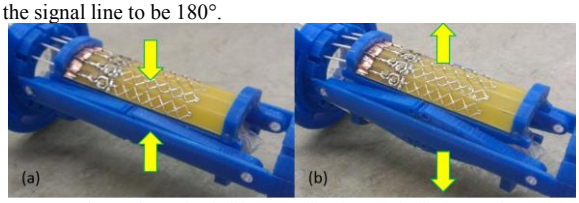


Figure 5. The scissor-jack-like mechanism of the transformable coil holder for the DPPX receive array can adapt to difference sizes of specimen. (a) position for the smallest speciman; (b) position for the largest specimen.

We incorporated switching connectors (R199006813, Radiall, Rosny-Sous-Bois, France) as shown in Fig 6. The internal mechanical switch of the switching connector directs the coil signal to the preamplifier by default; while it redirects the coil signal to the network analyzer when the external connector is plugged in. This allowed us to tune the DPPX coil without compromising the stability of the optimal length for preamp decoupling.

### *G. Linear birdcage transmit coil*

Ensuring equal and opposite flux induced in the two halves of the elements to achieve decoupling from the transmit field requires the element to be operating in a very homogeneous field. The trombone tuning design was used to ensure the homogeneity of the transmit coil used here [16]-[19]. A 60-mm diameter, 16-rung, high pass birdcage was constructed using ¼" and 3/16" laser-cut acrylic sheets. Each length-adjustable rung consisted of one fixed copper tube (ID/OD/Length: 0.125"/0.156"/3.8"; K&S Engineering, Chicago, IL, USA) and one mobile copper tube (OD/Length: 0.156"/3.8"; K&S Engineering) which were coupled together. To tune the frequency of the birdcage coil, one Nylon screw rod (1/2"-13) and two Nylon nuts (1/2"-13) were used to fine tune the length of the rungs.

### *H. Imaging*

Imaging experiments were carried out in the Varian Inova 4.7 T system. A cylindrical $CuSO_4$ phantom and a euthanized mouse were used to validate the decoupling between the adjacent DPPX receive elements and the coupling between DPPX coil and the transmit birdcage coil. Each imaging subject was loaded between the DPPX arrays first, and the arrays along with the imaging subject were inserted into the transmit birdcage coil together. The imaging parameters are shown in Table 1. Sum-of-squares was used to reconstruct the array image.

## III. Results & Discussion

The artifact of the loop mode formed by the return paths is illustrated in Fig 7(a-b). As shown in Fig 7(c), the DPPX trace, however, did not have any visible artifacts on the phantom image. The quasi-static B1 field of the DPPX coil was simulated and normalized as shown in Fig 8. The B1 field was mainly distributed on the bottom (signal-line side) of the coil as shown in Fig 8(b)-(e). The B1 field close to the DPPX coil was not homogenous along the long axis; however, the difference in imaging depth was fairly consistent, especially for the volume under the middle four crisscrossed loops.

During bench measurement, we found that the position of the transformable coil holder had very little effect on the tuning or matching of the DPPX coils or the birdcage coil. When the DPPX array was loaded with the $CuSO_4$ phantom and placed inside of the transmitting birdcage coil, the $S_{21}$ between each DPPX coil and the birdcage coil was -19 dB (for the DPPX coils on the sides of the array) to -54 dB (for the DPPX coils at the center of the array).

Phantom images are shown in Fig 9. The images received by the individual DPPX coils showed localized

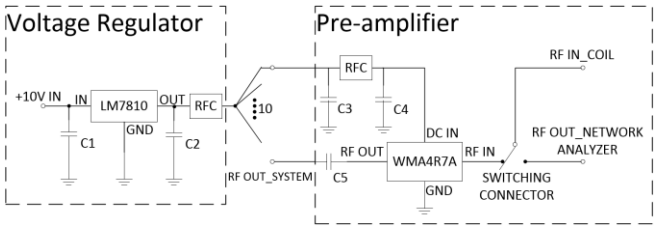


Figure 6. Voltage regulator, preamplifier and switching connector.

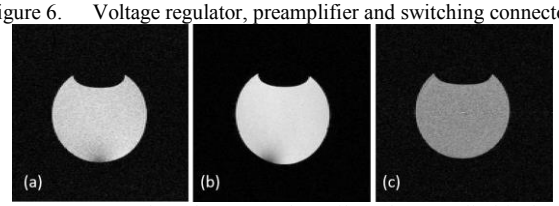


Figure 7. We taped each trace-only coil under a cylindrical $CuSO_4$ phatnom (OD = 27 mm, wall thickness = 300 μm), and we imaged the assembly inside of the transmitting birdcage coil. Because the wall thickness of the phantom was so thin and the coils were taped right on top of the phantom, any induced currents on the coils would de-phase the phantom signal and show shaded artifact on the image. Figure (a)-(c) show phantom images when (a) traditional DPP trace, (b) traditional DPP trace with shorted return path, and (c) DPPX trace were individually placed under the phantom.

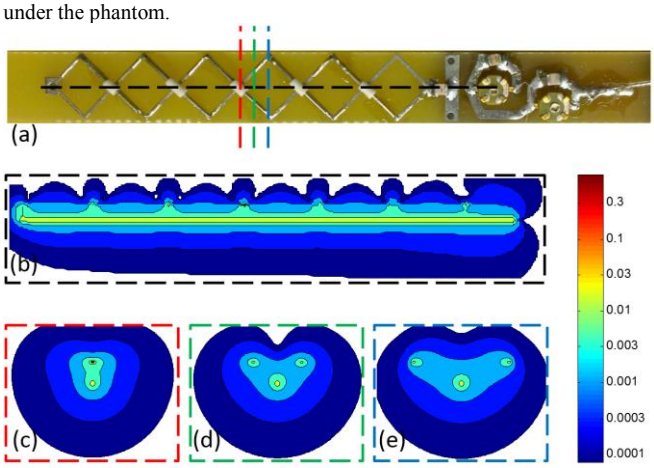


Figure 8. Contour plot of simulated B0 field. The B0 field was normalized to the maximum value inside of the 3-dimensional volume of interest. (a) The top side of the DPPX coil. Dashed lines were color coded to indicate the location of the B0 field at the (b) sagittal plane, and (c)-(e) different axial planes.

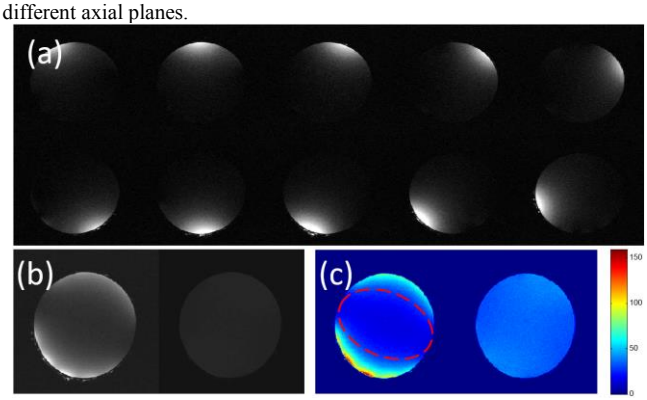


Figure 9. The CuSO4 phantom image was acquired by the DPPX array and the transmitting birdcage coil. (a) Phantom images acquired from individual DPPX coil. (b) (left) The composed array image using sum-of-square method. (b) (right) The volume image acquired by the birdcage coil when the DPPX array was inside of the birdcage coil (image intensity was increased by five times for visualization). (c) (left) The SNR of the sum-of-square image. (c) (right) The SNR map of the volume image. The red dashed line represens the SNR lower than the SNR received by the birdcage coil.

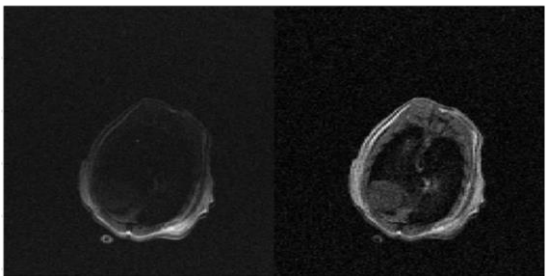

Figure 10. MR images of the mouse heart of the euthanized mouse. The image on the left shows the sum-of-square image received by the DPPX array. The image on the right shows the image received by the birdcage coil

imaging profiles as shown in Fig 9(a). The SNR comparison between the DPPX coil and the transmit birdcage coil is shown in Fig 9(c). As would be expected, the sum-of- square image showed high SNR = 160 on the outside of the phantom and decreased rapidly to SNR = 15 at the center of the phantom. The SNR of the volume-coil image showed consistent SNR = 35. The SNR inside of the sum-of-square image showed lower SNR than the volume coil, one indicator of high copper losses in the elements. The homogeneity of the transmit-coil image, as shown on the right of Fig. 9(b), with the array in place is worth noting as an indicator of a lack of interaction between the array and the transmit coil.

The MR images of a euthanized mouse are shown in Fig 10. Similar to the images of the $CuSO_4$ phantom, the SNR of the sum-of-square image was higher on the outside and lower at the inside of the euthanized mouse.

## IV. Conclusion

In summary, the array is extremely robust to loading conditions, compact, and mechanically adjustable to different sizes of specimen. The DPPX design successfully eliminated the coupling of the loop mode to the transmit coil as intended. Furthermore, the homogenous volume image of the phantom demonstrated that DPPX element is able to geometrically decouple from the transmit coil without the use of active-detuning circuits. The images received by individual DPPX array element also showed good decoupling between receive elements.

However, the copper losses from the DPPX elements will limit this particular array to use for surface applications. In addition, the characteristics of the element might prove useful when scaled to a larger size where sample loss dominance is more likely.

## Acknowledgment

The authors gratefully acknowledge support from the American Heart Association Grant No. 0930231N and technical supports from Dr. Steven Wright, Texas A&M University, Texas, USA. The MR images were acquired in Magnetic Resonance System Lab, Texas A&M University, Texas, USA.

## References

[1] P. Carmeliet, and D. Collen, "Transgenic mouse models in angiogenesis and cardiovascular disease," *The Journal of Pathology*, vol. 190, pp. 387-405, 2000.

[2] F.H. Epstein, "MR in mouse models of cardiac disease," *NMR in Biomedicine*, vol. 20, pp. 238-255, 2007.

[3] C.J. Goergen, K.N. Barr, D.T. Huynh, J.R. Eastham-Anderson, G. Choi, M. Hedehus, R.L. Dalman, A.J. Connolly, C.A. Taylor, P.S. Tsao, and J.M. Greve, "In vivo quantification of murine aortic cyclic strain, motion, and curvature: Implications for abdominal aortic aneurysm growth," *J. Magn Reson.*, vol. 32, pp. 847-858, 2010.

[4] J.L. Guenet, "Frontmatter," in *Standards of Mouse Model Phenotyping*, Wiley-VCH Verlag GmbH & Co. KGaA, 2008, pp. v-vi.

[5] J.E. Schneider, T. Lanz, H. Barnes, D. Medway, L.A. Stork, C.A. Lygate, S. Smart, M.A. Griswold, and S. Neubauer, "Ultra-fast and accurate assessment of cardiac function in rats using accelerated MRI at 9.4 Tesla," *Magn. Reson. Med.*, vol. 59, pp. 636-641, 2008.

[6] D. Gareis, T. Wichmann, T. Lanz, G. Melkus, M. Horn, and P.M. Jakob, "Mouse MRI using phased-array coils," *NMR in Biomedicine*, vol. 20, pp. 326-334, 2007.

[7] M.S. Ramirez, E. Esparza-Coss, and J.A. Bankson, "Multiple-Mouse MRI with Multiple Arrays of Receive Coils," *Magn. Reson. Med.*, vol. 63, pp. 803-810, 2010.

[8] O. Dietrich, T. Lanz, H.M. Reinl, B. Frank, M. Peller, M.F. Reiser, and S.O. Schoenberg, "Parallel imaging of mice on a clinical 3-telsa MRI system with a dedicated 8-channel small-animal coil array," *Proceedings of the 15th Annual Meeting of the ISMRM*, Berlin, Germany, 2007, pp. 1759.

[9] J.-X. WANG, N. Tian, F.J. Robb, A.P. Chen, L. Friesen-Waldner, B.K. Rutt, and C.A. McKenzie, "An 8-Channel Coil Array for Small Animal 13C MR Imaging," *Proceedings of the 18th Annual Meeting of the ISMRM*, Stockholm, Sweden, 2010, pp. 1489.

[10] T. Lanz, M. Müller, H. Barnes, S. Neubauer, and J.E. Schneider, "A high-throughput eight-channel probe head for murine MRI at 9.4 T," *Magn. Reson. Med.*, vol. 64, pp. 80-87, 2010.

[11] M. Tabbert, M. Motz, M. Lopez, E. Pfrommer, and S. Junge, "A 16-channel rat-body array coil with an integrated birdcage transmitter at 7T," *Proceedings of the 17th Annual Meeting of the ISMRM*, Honolulu, USA, 2010, pp. 4735.

[12] B. Keil, G.C. Wiggins, C. Triantafyllou, L.L. Wald, F.M. Meise, L.M. Schreiber, K.J. Klose, and J.T. Heverhagen, "A 20-channel receive-only mouse array coil for a 3 T clinical MRI system," *Magn. Reson. Med*., vol. 66, pp. 582-593, 2011.

[13] W. A. Edelstein, C. J. Hardy, and O. M. Mueller, "Electronic decoupling of surface-coil receivers for NMR imaging and spectroscopy," *J. Magn. Reson.*, vol. 67, pp. 156–161, 1986.

[14] P.B. Roemer, W.A. Edelstein WA, C. E. Hayes, S.P. Souza, O.M. Mueller, "The NMR phased array," *Magn. Reson. Med*., vol., 16 pp. 192–225, 1990.

[15] K.L. Moody, N.A. Hollingsworth, J.-F. Nielsen, D. Noll, S.M. Wright, and M.P. McDougall, "RF transparent array for testing multi-channel transmit systems," *Proceedings of the 18th Annual Meeting of the ISMRM*, Stockholm, Sweden, 2010.

[16] Y. Xu, and P. Tang, "Easy fabrication of a tunable high-pass birdcage resonator," *Magn. Reson. Med*., vol. 38, pp. 168-172, 1997.

[17] M.P. McDougall, S.M. Wright, and D.G. Brown, "A low-pass trombone birdcage coil with broad tuning range," *Proceedings of the 9th Annual Meeting of the ISMRM*, Glasgow, Scotland, UK, 2001, pp. 18.

[18] J.M. Jin, *Electromagnetic analysis and design in magnetic resonance imaging*, CRC Press, 1999.

[19] D.K. Spence, and S.M. Wright, "2-D full wave solution for the analysis and design of birdcage coils," Concepts in Magnetic Resonance Part B: Magnetic Resonance Engineering, vol. 18B, pp. 15-23, 2003.